ACS OMEGA

http://pubs.acs.org/journal/acsodf

Article

Hydrophobic Magnetic Porous Material of *Eichhornia crassipes* for Highly Efficient Oil Adsorption and Separation

Ruikun Sun, Lei He, Qingtong Shang, Shiqi Jiang, Chunxia Zhou, Pengzhi Hong, Hui Zhao, Shengli Sun, and Chengyong Li*

Cite This: *ACS Omega* 2020, 5, 9920−9928

Read Online

ACCESS | Metrics & More | Article Recommendations | Supporting Information

ABSTRACT: Many oil adsorption materials are composed of nonrenewable raw materials, and their disposal can increase resource consumption and cause new environmental pollution. In this paper, the carbonized *Eichhornia crassipes* (CEC) were immobilized with Fe_3O_4 magnetic nanoparticles and modified with 1*H*, 1*H*, 2*H*, 2*H*-perfluorooctyltriethoxysilane (PFOS) to prepare an oil adsorption material, referred to here as CEC/Fe_3O_4/PFOS. The magnetic and mechanical strength of the CEC was enhanced by adding Fe_3O_4 magnetic particles, which enable it efficient to dispose the oil/water solution. CEC/Fe_3O_4/PFOS shows high porosity (83.53%), low skeletal density (0.487 g/cm^3), excellent magnetism, ultrahigh oil absorption capacity (49.94−140.90 g/g), hydrophobic performances with a water contact angle of 150.1 ± 2.3°, and a sliding angle of 10.5°. It is worth noting that the material can be recycled, and the absorbed oil is obtained by distillation. Therefore, this work may provide a candidate for solving the problem of oil pollution using *E. crassipes*.

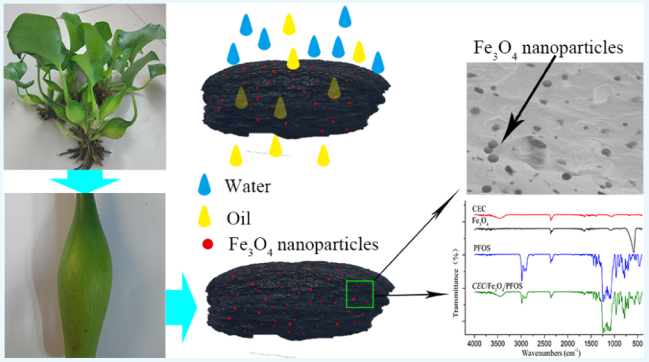

1. INTRODUCTION

The leakage of petroleum and the waste oil discharge from oil manufactures and domestic sewage have caused severe environmental pollution. The causes of oil pollution are various, including petroleum leakage, waste oil discharge during factory production and processing, edible oil in domestic sewage, etc.[1,2] Till now, the treatment of oil pollution commonly includes burning and collecting. Among them, burning is not desirable due to the generation of additional pollution. However, compared to the former, the collecting method has the advantages of easy recovery of the oil, no secondary pollution, and high purifying efficiency. Hydrophobic sponges handle oil spills by absorbing oil in water, and sponges can be recycled by squeezing or distillation.[2] Besides, the perfect adsorption material should exhibit big adsorption space, which has high adsorption rate and superhydrophobic capacity.

The characteristics of the hydrophobic surface are the prerequisites for efficient adsorption materials, such as single crystalline silicon,[3] polydimethylsioxane (PDMS) membranes,[4] and polytetrafluoroethylene.[5] Moreover, the construction of the hydrophobic surface can be achieved by increasing the surface roughness or modified with the coating of hydrophobic materials[6−9] such as cellulose[8] and carbon fiber aerogels (CFAs), which was reported using natural sisal as a raw material. The surface of CFAs is hydrophobically modified with 3-methacryloxypropyltrimethoxysilane (KH570). In addition, the advantages of the CFA material include elasticity, highly recyclable superhydrophobicity, low density, and high porosity. The porosity of the porous structure has been considered to be another requirement for becoming an excellent adsorption material. Biomass carbon is a porous material with relatively low density and a large specific area.[10] The advantages of biomass carbon such as high adsorption rate, cheap production cost, and easy manipulation are verified during the oil adsorption process. Hence, biomass carbons have attracted the interest of the technician, leading to the development of different kinds of biomass carbon materials.[11−13] In fact, the low mechanical and poor dimensional stability of most biomass carbons cannot make them to be utilized as oil adsorption materials to absorb waste oil and separate the oil/water solution.[14,15] However, these defects can be improved in degree by adding nanoparticles.[12,16,17]

Eichhornia crassipes (E.C.) are widely distributed in the subtropical region. They tend to grow in warm-humid environments uch as ponds, ditches, and rice fields (Figure 1a),[18,19] and they grow unlimitedly through asexual propagation and form new ramets from axillary buds on stolon (Figure 1b).[20]

Received: January 15, 2020
Accepted: April 9, 2020
Published: April 21, 2020

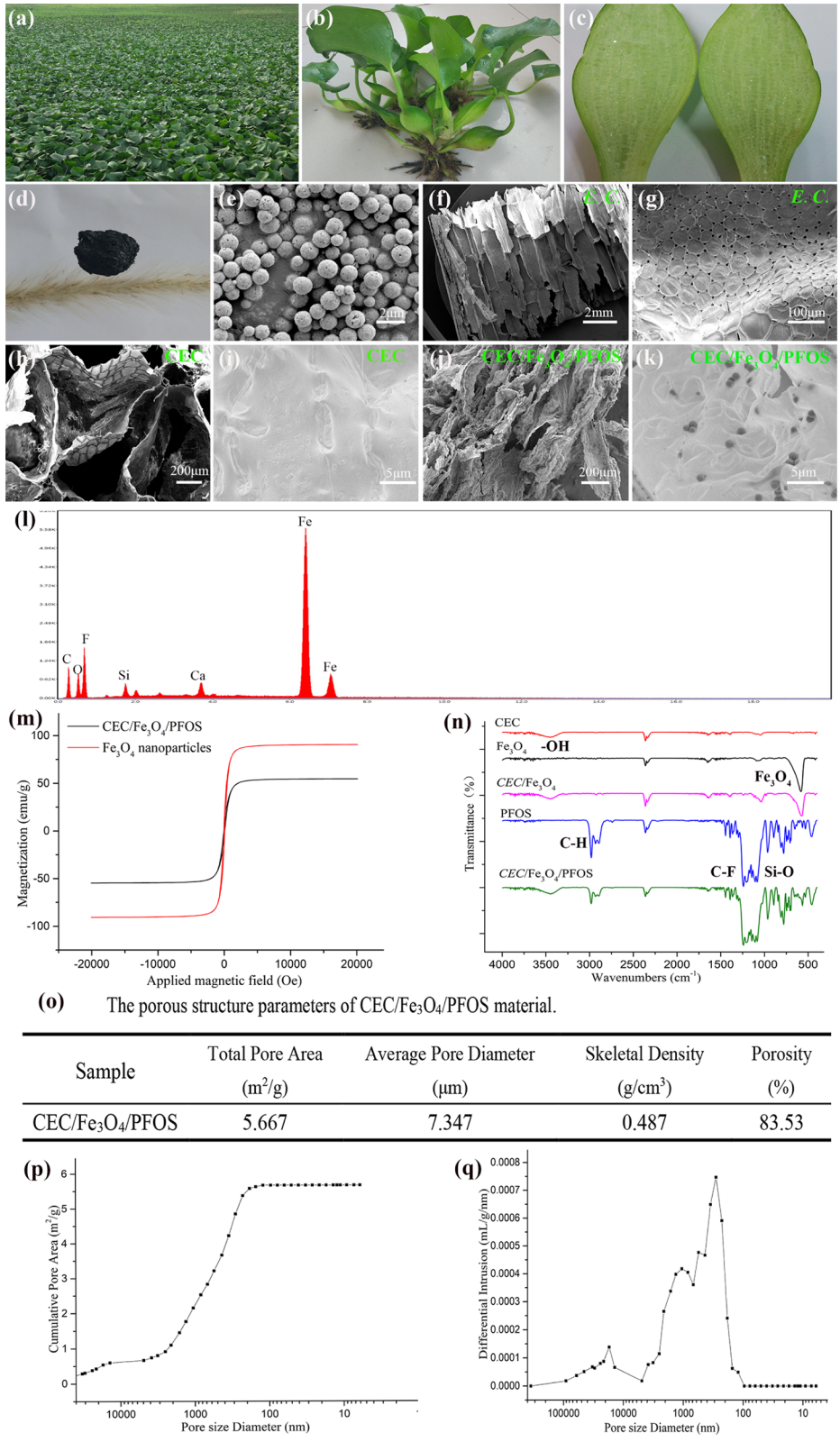

(o) The porous structure parameters of $CEC/Fe_3O_4/PFOS$ material.

Sample	Total Pore Area (m^2/g)	Average Pore Diameter (μm)	Skeletal Density (g/cm^3)	Porosity (%)
$CEC/Fe_3O_4/PFOS$	5.667	7.347	0.487	83.53

Figure 1. Characterization of samples. (a) Community of E.C. (b) Plant of E.C. (c) Porous structure of E.C. (d) Digital image of the $CEC/Fe_3O_4/PFOS$ material. (e) Scanning electron microscopy (SEM) morphologies of Fe_3O_4 magnetite particles. (f, g) SEM morphologies of E.C. at different magnifications. (h, i) SEM morphologies of carbonized *Eichhornia crassipes* (CEC) at different magnifications. (j, k) SEM morphologies of the $CEC/Fe_3O_4/PFOS$ material at different magnifications. (l) Energy dispersive spectroscopy (EDS) recorded analysis of the $CEC/Fe_3O_4/PFOS$ material. (m) Magnetization curves of Fe_3O_4 nanoparticles and the $CEC/Fe_3O_4/PFOS$ material. (n) Fourier transform infrared spectroscope (FT-IR) spectra of CEC, Fe_3O_4 magnetite particles, perfluorooctyltriethoxysilane (PFOS), CEC/Fe_3O_4, and $CEC/Fe_3O_4/PFOS$ material. (o) Porous structure parameters of the $CEC/Fe_3O_4/PFOS$ material. (p) Cumulative pore area of the $CEC/Fe_3O_4/PFOS$ material. (q) Pore size distribution water separation material curve of the $CEC/Fe_3O_4/PFOS$ material.

https://dx.doi.org/10.1021/acsomega.0c00200
ACS Omega 2020, 5, 9920−9928

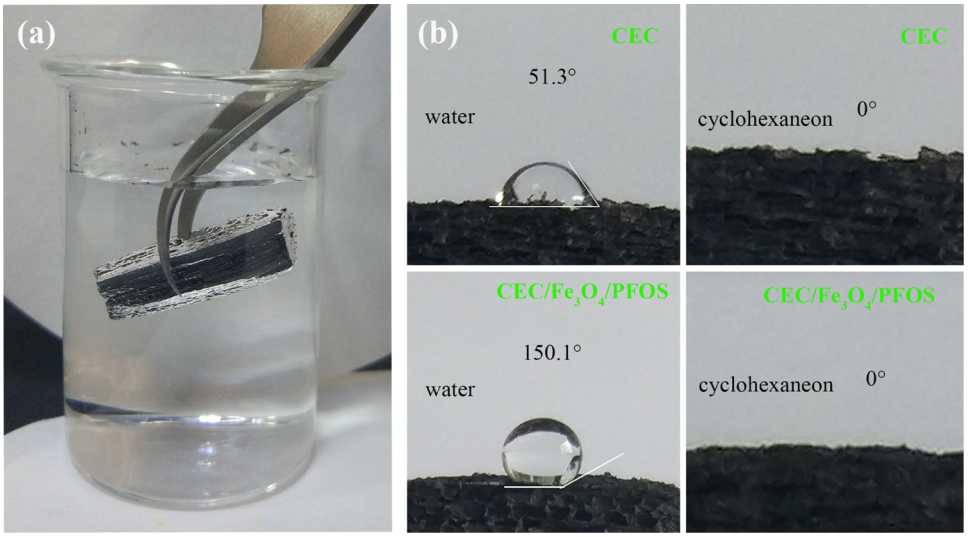

Figure 2. Surface performances of the material. (a) Digital image of the CEC/Fe_3O_4/PFOS material immersed in water by force. (b) Contact angle measurements for the CEC and CEC/Fe_3O_4/PFOS material.

Dense E.C. communities threaten to lead to certain negative effects, including (1) hampering the shipping; (2) reducing the dissolved oxygen levels and nutrients; (3) declining the production of aquatic products; and (4) deteriorating water quality and threatening human health.[21−23] However, recent research indicates that the bleached E.C. is an efficient adsorbent for the cationic dyes.[24] Due to the porous structure of E.C., the result shows that the maximum removal capacity for Zn, Cu, and Cd with E.C. is reached at pH 5.[25]

In this work, we report a simple immersion method to prepare an oil/water separation material (CEC/Fe_3O_4/PFOS) through the surface immobilization of Fe_3O_4 magnetic nanoparticles and hydrophobic modification with PFOS. The CEC/Fe_3O_4/PFOS material shows high porosity, low skeletal density, excellent magnetism, hydrophobic performances, and lipophilic ability. It is expected that the preparation of CEC/Fe_3O_4/PFOS will become a promising candidate for an oil/water separation material.

2. RESULTS

2.1. Characterization of the CEC/Fe_3O_4/PFOS Material.

Figure 1a−c shows the growth environment and porous structure of E.C. The porous structure of E.C. is suitable for the preparation of oil/water separation materials. Figure 1d shows the digital image of the prepared CEC/Fe_3O_4/PFOS material. Figure 1e shows the morphologies of the Fe_3O_4 magnetite particles. Fe_3O_4 magnetite particles with an average diameter of approximately 800 nm were obtained, as revealed by scanning electron microscope (SEM) images. Figure 1f−g shows the porous structure of E.C., and many micropores are presented on the skeleton. Figure 1h−k shows the morphologies of the CEC and CEC/Fe_3O_4/PFOS material. It is noted that for the CEC/Fe_3O_4/PFOS material, the content of the PFOS ethanol solution was maintained at 2.5 wt % and 1 mg/mL of Fe_3O_4 ethanol solution was added if there was no additional illustration. It is clearly seen that there are mass of micro nanopores in the CEC and CEC/Fe_3O_4/PFOS material. When E.C. was carbonized, the micro gap appeared on the carbon skeleton of E.C. The characteristics of the micro gap are influenced by carbonization temperature, heating rate, and carbonization time.[26] The carbon skeleton surface of the CEC/Fe_3O_4/PFOS material was observed by SEM. It can be clearly seen from the screen that the black dot-shaped Fe_3O_4 magnetite particles are uniformly dispersed on the surface of the carbon skeleton (Figure S2a). Figure S2b shows the size of Fe_3O_4 magnetite particles on the CEC/Fe_3O_4/PFOS material surface. The energy dispersive X-ray (EDX) spectrum of the CEC/Fe_3O_4/PFOS material (Figure 1i) demonstrates that the as-prepared CEC/Fe_3O_4/PFOS material possesses Fe, Si, and F elements. The results indicated that Fe_3O_4 is successfully deposited and hydrophobically modified by PFOS. Figure 1m shows the magnetic properties of the original Fe_3O_4 nanoparticles and CEC/Fe_3O_4/PFOS material. Both Fe_3O_4 nanoparticles and CEC/Fe_3O_4/PFOS material show obvious superparamagnetism. By analyzing the relationship between Fe_3O_4 nanoparticles and CEC/Fe_3O_4/PFOS material and magnetic field, it is clearly seen that the responses of Fe_3O_4 nanoparticles and CEC/Fe_3O_4/PFOS material are linearly related to the magnetic fields, but basically stable at high field intensity. When the magnetic field is removed, they present standard paramagnetic characteristics without exhibiting hysteresis. Compared with Fe_3O_4 nanoparticles (90.67 emu/g), the CEC/Fe_3O_4/PFOS material shows lower magnetization (54.63 emu/g). Under the effect of an external magnetic field, the CEC/Fe_3O_4/PFOS material still has responsiveness. As shown in Figure 1n, the chemical features of the CEC, Fe_3O_4 magnetite particles, PFOS, CEC/Fe_3O_4, and CEC/Fe_3O_4/PFOS material were characterized using the Fourier transform infrared spectroscope (FT-IR). The wide absorption band of CEC located at 3450 cm^{-1} is attributed to the stretching vibrations of −OH, demonstrating that the CEC surface is inherently hydrophilic.[27] It is believed that the peaks at 579 cm^{-1} represent the characteristic absorption peaks of Fe_3O_4 magnetite particles.[28] The absorption bands of PFOS at 3034−2809, 1272−1147, and 1091−987 cm^{-1} correspond to the stretching vibrations of the C−H, C−F, and Si−O bonds, respectively.[29,30] The stretching vibration band at 2900 cm^{-1} is attributed to C−H groups. These results confirm the presence of methyl and methylene groups in PFOS. Moreover, in the spectra of PFOS, the peak at 1200 cm^{-1} is attributed to the stretching vibration of C−F, while the peak at 1053 cm^{-1} is assigned to the presence of the Si−O bond. The above observation illustrated that PFOS

https://dx.doi.org/10.1021/acsomega.0c00200
ACS Omega 2020, 5, 9920−9928

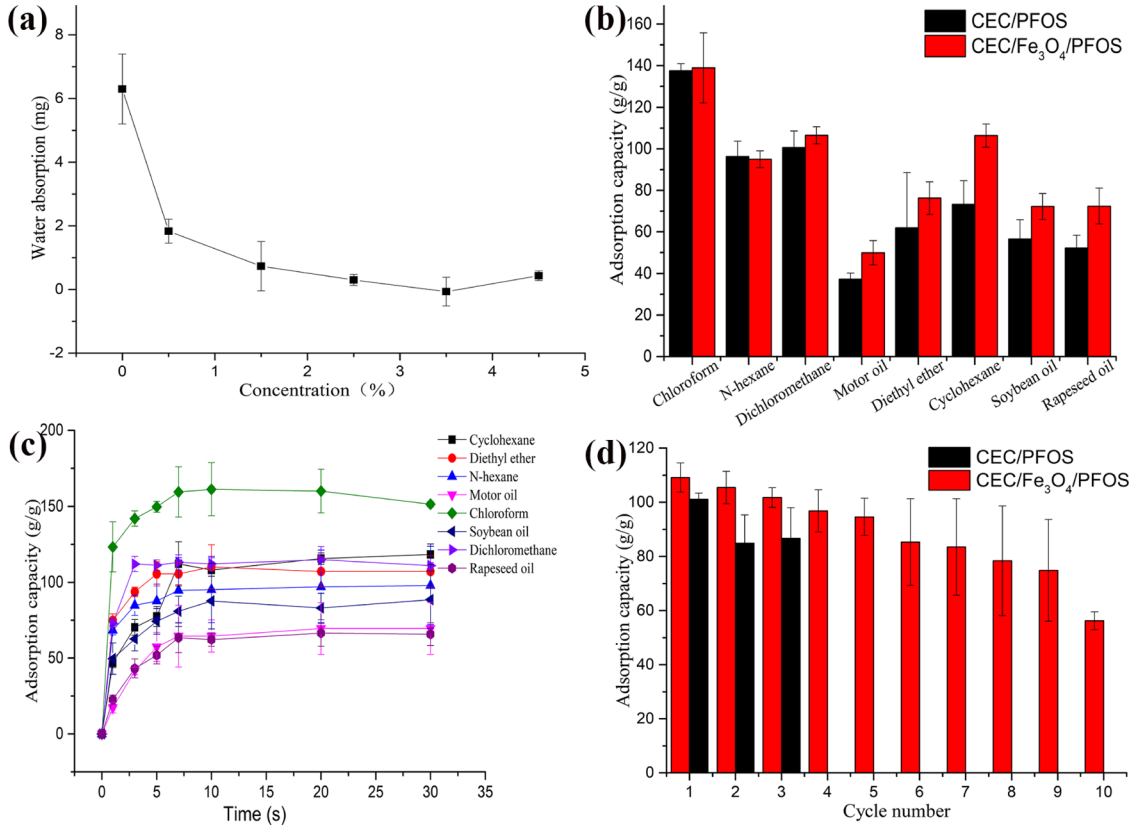

Figure 3. Adsorption performance of the material. (a) Variation of the water adsorption capacity of the CEC/Fe_3O_4/PFOS material with increasing PFOS concentration. (b) Adsorption capacity of the CEC/PFOS material and CEC/Fe_3O_4/PFOS material toward eight different oils (trichloromethane, *n*-hexane, dichloromethane, engine oil, ether, cyclohexane, soybean oil, rapeseed oil). (c) Absorption kinetics for eight different oils of the CEC/Fe_3O_4/PFOS material. (d) Changes in material adsorption capacity with the number of adsorption measurement cycles.

belongs to the perfluorosilane reagent. After the modification of Fe_3O_4 magnetite particles and PFOS, several absorption peaks of Fe_3O_4 magnetite particles and PFOS appear on the modified CEC surfaces. All of these results confirm that the obtained perfluorooctyl chains and Fe_3O_4 magnetite particles have been successfully fixed to the CEC surfaces, which is favorable for the hydrophobicity of the CEC/Fe_3O_4/PFOS material. Furthermore, Figure 1o shows the porous structure parameters of the CEC/Fe_3O_4/PFOS material. The measured MIP total pore area, average pore diameter, skeletal density, and porosity of the CEC/Fe_3O_4/PFOS material is 5.667 m^2/g, 7.347 μm, 0.487 g/cm^3, and 83.53%, respectively. Figure 1p shows the relation between the cumulative pore area and pore size diameter of the CEC/Fe_3O_4/PFOS material. When the pore size is between 45−350 and 0.2−1 μm, the cumulative pore area increases. Moreover, the cumulative pore area of 0.2−1 μm increases faster. It indicates that small-sized holes (0.2−1 μm) account for the majority of all holes. As shown in Figure 1q, the pore size of the CEC/Fe_3O_4/PFOS material is mainly distributed between 0.2 and 90 μm. Comparing the results of Figure 1p and Figure 1q, it is seen that there are both large pores (45−90 μm) and small pores (0.2−1 μm) on the inner surface of the CEC/Fe_3O_4/PFOS material, but the majority is small pores.

2.2. Surface Performances Measurements. When the CEC/Fe_3O_4/PFOS material is immersed in water with outside intervention, the air remaining on the surface of the material and the surrounding water can form an interface. The formation of a mirror-like surface on the CEC/Fe_3O_4/PFOS material can be observed with the naked eye, which can be attributed to the Cassie−Baxter nonwetting behavior (Figure 2a).[31] Distilled water and cyclohexane were used as probe liquids to investigate the hydrophobic and lipophilic performance of the CEC/Fe_3O_4/PFOS material. Figure 2b shows that the water contact angle at three different positions of CEC is 51.3 ± 1.7°. The result is in agreement with other literature.[32] Compared with CEC, the water contact angle at three different positions of the CEC/Fe_3O_4/PFOS material is substantially increased to 150.1 ± 2.3°. The results indicate that the surface hydrophobicity of the material increases obviously. Figure S3 shows the water sliding angles and static contact angles of the CEC/Fe_3O_4/PFOS material are 10.5 and 146.9°, respectively. Besides, both CEC and CEC/Fe_3O_4/PFOS material show the excellent cyclohexane wettability and 0° contact angle, and the material surface is uninfluenced with the lipophilic feature. Specifically, for the surface of the CEC/Fe_3O_4/PFOS material, when water was dropped, the droplets quickly glided over. Movie S1 records the whole dynamic processes, which proves its remarkable hydrophobic properties.

2.3. Oil Adsorption Measurement and Evaluation. The CEC/Fe_3O_4/PFOS material was modified by the concentration of the PFOS ethanol solution (0.5, 1.5, 2.5, 3.5, 4.5 wt %). The CEC/Fe_3O_4/PFOS material modified with different concentrations of PFOS was dropped in the same volume of water. A little water can be absorbed by the CEC/Fe_3O_4/PFOS material because of the incomplete coverage of perfluorooctyl chains on the material. The water adsorption capacity is calculated according to the weight differences of the material before and after adsorbing water. Figure 3a shows the water adsorption

https://dx.doi.org/10.1021/acsomega.0c00200
ACS Omega 2020, 5, 9920−9928

capacity of the CEC/Fe_3O_4/PFOS material with different concentrations of PFOS. The water absorption capacity of CEC/Fe_3O_4/PFOS materials decreases with the increase of the PFOS concentration (0−2.5 wt %). When the concentration of PFOS exceeds 2.5 wt %, the adsorption capacity of CEC/Fe_3O_4/PFOS materials is almost unchanged. Therefore, the concentration of PFOS was selected to be 2.5% in subsequent experiments.

The adsorption ability of the CEC/PFOS material and the CEC/Fe_3O_4/PFOS material toward eight different oils and organic reagents is shown in Figure 3b. It is obviously shown that the eight kinds of oils or organic solvents, CEC/Fe_3O_4/PFOS material, and CEC/PFOS material display the highest adsorption capacity for trichloromethane and the lowest adsorption capacity for engine oil. The adsorption capacities of CEC/Fe_3O_4/PFOS material are different for eight oils or organic reagents (from 49.97 to 140.90 g/g). The reason for the different adsorption capacities of the CEC/Fe_3O_4/PFOS material is that adsorption solutions have different viscosities. The adsorption capacity of the CEC/Fe_3O_4/PFOS material is higher than that of the CEC/PFOS material because the adsorption capacity of the CEC/Fe_3O_4/PFOS material is increased through the addition to Fe_3O_4 nanoparticles. The absorption mechanism of the CEC/Fe_3O_4/PFOS material may be attributed to the following. The physical adsorption can be a significant part in the adsorption experiments. When the CEC/Fe_3O_4/PFOS material is in touch with oils or organic reagents, the oils or organic reagents will be stored in the hydrophobic material by force.[33] The force is made up of capillary effects and hydrophobic interaction.[34,35]

The absorption kinetics for the CEC/Fe_3O_4/PFOS material with different oils or organic solvents are presented in Figure 3c. The CEC/Fe_3O_4/PFOS material has different absorption capacities and time for diverse oils and organic reagents. The absorption saturation of dichloromethane was the fastest in 3 s, and the absorption saturation of others was achieved in less than 7 s. The reason for the time of adsorption saturation is that adsorption solutions have different viscosities and fluidities. Figure 3d shows the adsorption capacity of the CEC/PFOS material, and the CEC/Fe_3O_4/PFOS material was measured with different cycle numbers. The materials full of oils were reused by the distillation method. After three adsorption cycles, the result shows that the absorption volume of the CEC/Fe_3O_4/PFOS material cannot be influenced obviously. The image shows that the structure of the CEC/Fe_3O_4/PFOS material is intact in Figure S4a. Due to the low mechanical strength, the CEC/PFOS material is disrupted after three adsorption cycles. The image shows that the structure of the CEC/PFOS material is disrupted in Figure S4b. In addition, the absorption capacity result of the ninth repeatable cycle is close to 80% of the original value, but the adsorption capacity decreases after the 10th repeatable cycle.

Table 1 shows the comparison of the adsorption capacity of the CEC/Fe_3O_4/PFOS material in this work and the different materials in the literature. The adsorption capacity of the CEC/Fe_3O_4/PFOS material is higher than that of other materials of biomass charcoal. But only the adsorption capacity of an aerogel material is higher than that of the CEC/Fe_3O_4/PFOS material. Due to the extremely low density of aerogel materials, most of the cellulose is used as the adsorbent but the raw materials of the plant as an oil adsorbent material have been seldom. Lee et al.[44] made a magnetic adsorption material (MS-PDMS) by sponges and Fe_3O_4 nanoparticles; the material shows the oil/water separation ability and adsorption ability (34.8−37.9 g/g). Compared with MS-PDMS, the CEC/Fe_3O_4/PFOS material provides significant advancement in the oil/water separation application. The oil adsorption capacity (49.97−140.90 g/g) of the CEC/Fe_3O_4/PFOS material is much better than MS-PDMS samples (34.8−37.9 g/g), so it is efficient for oil−water separation. The CEC/Fe_3O_4/PFOS material has a higher water contact angle (150.1°) than the PLA/γ-Fe_2O_3 composite membranes (148°) and MS-PDMS samples (141°).[41,44] Compared with the nanoparticles of PLA/γ-Fe_2O_3 composite membranes, the Fe_3O_4 nanoparticles of the CEC/Fe_3O_4/PFOS material not only enhance the roughness and mechanical strength of the material, but also make the material magnetic, which is convenient for the magnet-controlled oil−water separation. Finally, the raw materials of the CEC/Fe_3O_4/PFOS material are invasive plants. Compared with PLA membranes and sponges, invasive plants have no chemical reaction during the preparation process, which reduces environmental pollution and harm to invasive plants.

Table 1. Adsorption Capacities Comparison of the CEC/Fe_3O_4/PFOS Material in This Work and Different Materials in the Literature

adsorption material	type of use	adsorption capacity (g/g)	literature
hollow carbon spheres	adsorption oils	10	36
cellulose hybrid biomembrane	oil/water separation	5−20	37
hybrid aerogels derived	oil/water separation	35−115	38
cellulose-based aerogels	oil/water separation	58.06−101.14	39
lignin modified aerogel	oil/water separation	20−40	40
polylactic acid (PLA) foam	oil/water separation	14−34	41
biomass carbon@SiO_2@MnO_2 aerogel	oil/water separation	60−120	12
carbon microbelt aerogel	oil/water separation	56−188	42
carbon fiber aerogel	oil/water separation	50−192	43
MS-PDMS	oil/water separation	34.8−37.9	44
CEC/Fe_3O_4/PFOS material	oil/water separation	49.97−140.90	this work

2.4. Oil/Water Separation Performance. The CEC/Fe_3O_4/PFOS material shows the hydrophobic, lipophilic, and excellent oil adsorption capacities. To provide accurate research of the CEC/Fe_3O_4/PFOS material, qualitative evaluation and quantitative measurements of oil adsorption capacity were measured. In Figure 4a, Sudan III is used as an indicator to stain trichloromethane. Since the density of trichloromethane is higher than water, the trichloromethane droplet sunk down to water. The stained trichloromethane represents oil pollution in adsorption experiments. The CEC/Fe_3O_4/PFOS material is fixed by a plastic pipe, keeping it in contact with trichloromethane droplets. It is clearly seen that the trichloromethane is quickly absorbed by the CEC/Fe_3O_4/PFOS material. In about 7 s, the underwater trichloromethane is entirely absorbed by the CEC/Fe_3O_4/PFOS material. Movie S2 shows the whole process of the adsorbed underwater trichloromethane experiments. Similarly, due to the density of cyclohexane being lower than water, the cyclohexane floats on the surface of water. The stained cyclohexane represents oil pollution in adsorption experiments

https://dx.doi.org/10.1021/acsomega.0c00200
ACS Omega 2020, 5, 9920−9928

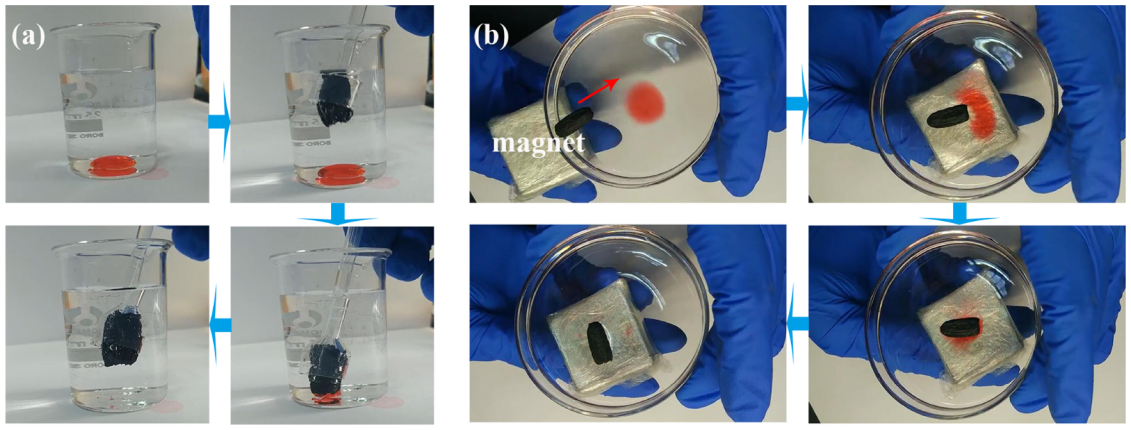

Figure 4. Oil adsorption ability of the material. (a) Oil adsorption ability of the CEC/Fe_3O_4/PFOS material toward trichloromethane. (b) Oil adsorption ability of the CEC/Fe_3O_4/PFOS material toward cyclohexane.

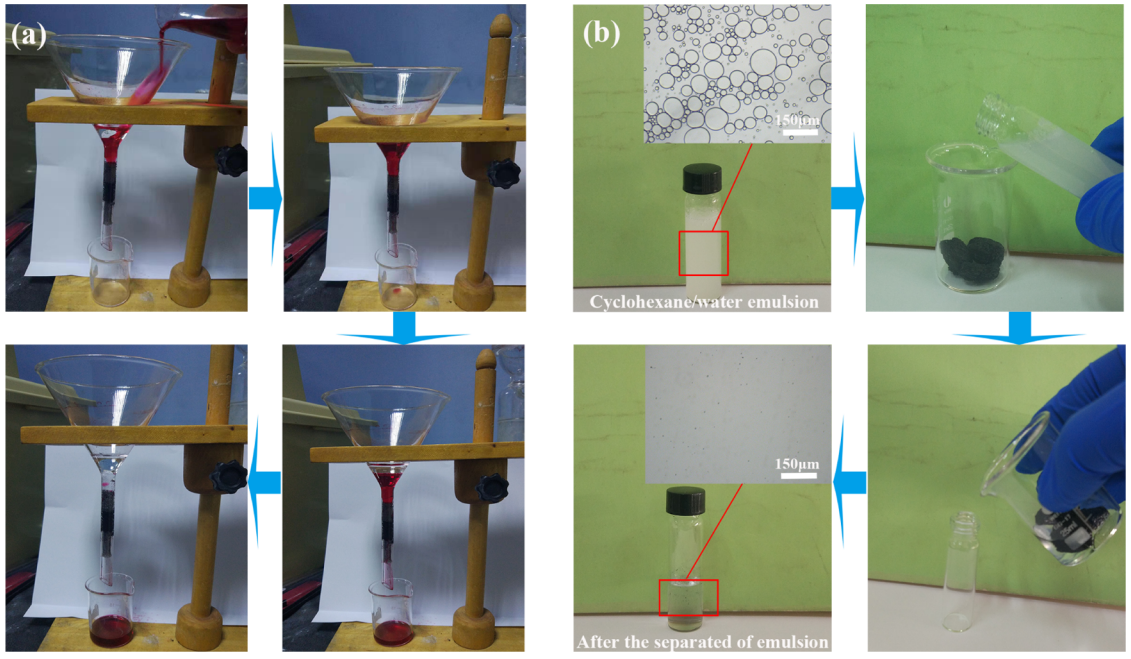

Figure 5. Oil separating ability of the material. (a) Trichloromethane/water mixed solution was separated by the CEC/Fe_3O_4/PFOS material as the filter material. (b) Cyclohexane/water emulsion was separated by the CEC/Fe_3O_4/PFOS material.

(Figure 4b). The CEC/Fe_3O_4/PFOS material is controlled by a magnet to approach the floating cyclohexane. As shown in Movie S3, the stained cyclohexane is absorbed by the CEC/Fe_3O_4/PFOS material, which still floats on the surface of the water without sinking. The results p3 oily wastewater treatment.

Benefiting from the hydrophobicity and lipophilicity of the CEC/Fe_3O_4/PFOS material, the entry of water is resisted but oil is allowed to pass through. These properties indicate that the CEC/Fe_3O_4/PFOS material can be used as a separation device for treating the oil/water mixed solution and the oil/water emulsion. Here are two different methods to explore the separated mixed solution of the CEC/Fe_3O_4/PFOS material. One of the strategies is to separate the oil/water mixture by gravity driven and the other is to separate the oil/water emulsion through the adsorption performance.

The separation device is shown in Figure S5. The trichloromethane/water mixture solution is separated by the CEC/Fe_3O_4/PFOS material. The photographs in Figure 5a also display the separation of the trichloromethane/water mixed solution. At first, the trichloromethane/water mixed solution was poured in a funnel. During trichloromethane/water separation, trichloromethane penetrates into the CEC/Fe_3O_4/PFOS material by gravity driven, and water is trapped by the funnel. Obviously, trichloromethane from the mixed solution is collected in a beaker. The above oil/water separation clearly shows that the CEC/Fe_3O_4/PFOS material is an ideal separation material. In summary, the CEC/Fe_3O_4/PFOS material shows high oil and organic reagent adsorption capability and excellent trichloromethane/water separation capability. Figure 5b shows the cyclohexane/water emulsion separated by the CEC/Fe_3O_4/PFOS material. The cyclohexane/water emulsion is milky and opaque. The emulsion was poured into a beaker containing the CEC/Fe_3O_4/PFOS material. After the CEC/Fe_3O_4/PFOS material was immersed and kept for 30 s, the emulsion became transparent. The cyclohexane/water emulsion before and after separation was observed by an optical microscope. The results show that there are many droplets (5−97 μm) in the microscope's field before

https://dx.doi.org/10.1021/acsomega.0c00200
ACS Omega 2020, 5, 9920−9928

the cyclohexane is adsorbed by the CEC/Fe_3O_4/PFOS material. After the solution is separated, only a few small oil droplets are observed in the microscope's field. This also proves that the CEC/Fe_3O_4/PFOS material possesses excellent purification and adsorption abilities in the water.

3. CONCLUSIONS

In this work, we report a simple immersion method to prepare an oil/water separation material (CEC/Fe_3O_4/PFOS) through surface immobilization of Fe_3O_4 magnetic nanoparticles and hydrophobic modification with PFOS. Fe_3O_4 particles evenly disperse on the skeleton and enhance the mechanical strength of the material. The CEC/Fe_3O_4/PFOS material shows high porosity (83.53%), low skeletal density (0.487 g/cm^3), excellent magnetism, hydrophobic performances with a water contact angle of 150.1 ± 2.3°, sliding angle of 10.5°, and lipophilic ability with a cyclohexane contact angle of 0°. The porous structure endows the CEC/Fe_3O_4/PFOS material with ultrahigh oil adsorption capacity (49.94−140.90 g/g) and oil/water separation ability. Even for the oil/water emulsion, the material has good separation ability. Therefore, this work reduces the influence of invasive plants and solves the problem of oil pollution using E.C.

4. EXPERIMENTAL PROCESS

4.1. Materials. E.C. was harvested from the waterways of Zhanjiang (Guangdong, China). 1*H*, 1*H*, 2*H*, 2*H*-perfluorooctyltriethoxysilane (PFOS, 99.0%) were obtained from Shanghai Macklin Bio-chemical Technology Co., Ltd. (Shanghai, China). Analytical reagent grade of ferric chloride hexahydrate, Sudan III, ethylene glycol, sodium acetate trihydrate, ethanol, and other chemicals were purchased from Guangzhou Binshang Biotechnology Co., Ltd. (Guangzhou, China).

4.2. Synthesis of Fe_3O_4 Magnetite Particles. The magnetite particles with a mean diameter of 800 nm were prepared. First, 5.2 g of $FeCl_3{\cdot}6H_2O$ and 11.5 g of sodium acetate were dissolved in 100 mL of ethanol solution, and the solution was stirred at 900 rpm for 30 min. Then the solution was transferred to a hydrothermal reactor. The hydrothermal reactor was heated to 200 °C at a rate of 10 °C/min and kept for 8 h, and then cooled to 25 °C. The acquired magnetite nanoparticles were rinsed with absolute ethanol. Finally, the Fe_3O_4 magnetite nanoparticles were vacuum dried at 60 °C.

4.3. Preparation of Carbonaceous E.C. Carbonization was utilized to prepare CEC. Fresh stem of E.C. was washed with distilled water and stored at −76 °C for 2 days, and then freeze-dried at −48 °C under vacuum for 24 h. Subsequently, the dried stem was carbonized by a high-temperature tube furnace. To avoid oxygen participation during the carbonization, the tube furnace was kept in vacuum and charged at a rate of 9 sccm with nitrogen. The high-temperature tube furnace heated the material to 900 °C at a rate of 5 °C/min and kept for 2 h. Finally, the CEC material was cooled to 25 °C.

4.4. Preparation of Magnetic CEC. Twenty milligrams of Fe_3O_4 magnetic particles were dispersed in 20 mL of ethanol by sonication. Then, 2 mL of the mixture was dropped onto the surface of each CEC (6−8 mm in diameter and 2−3 cm in height) to allow Fe_3O_4 magnetic particles to enter the porous structure of the CEC. Next, the CEC material was placed at 25 °C for 8 h, keeping its porous structure in strong contact with the Fe_3O_4 magnetic particle solution. Finally, ethanol in the magnetic carbonaceous E.C. was removed by vacuum drying at 45 °C for 8 h.

4.5. Preparation of Hydrophobic CEC/Fe_3O_4. Each CEC/Fe_3O_4 material was modified using 5 mL of the PFOS ethanol solution. CEC/Fe_3O_4 was immersed in different amounts of the PFOS ethanol solution for 8 h. Correspondingly, the content of PFOS ethanol solution was 0.5, 1.5, 2.5, 3.5, and 4.5 wt %. Finally, the hydrophobic CEC/Fe_3O_4/PFOS was washed with ethanol and vacuum dried at 45 °C for 8 h. The porous structure and surface hydrophobicity of the material were improved, and the morphology was not changed.

4.6. Oil Adsorption Measurements. First, the CEC/Fe_3O_4/PFOS material was dipped in different oils and organic reagents for 3 min. After that, the CEC/Fe_3O_4/PFOS material was taken out and the solution on the CEC/Fe_3O_4/PFOS material surface was removed by filter paper. Next, the weights of the CEC/Fe_3O_4/PFOS material were recorded by an analytical balance. The adsorption volume of the CEC/Fe_3O_4/PFOS material was measured according to the formula

$$Q = \frac{m_2 - m_1}{m_1} \quad (1)$$

where m_1 is the weight of the CEC/Fe_3O_4/PFOS material, m_2 is the weight of the CEC/Fe_3O_4/PFOS material after adsorbing oils or organic reagent. After the adsorption test, the CEC/Fe_3O_4/PFOS material was measured for eight oils or organic reagents. After the cycle adsorption test, the cyclohexane in the material was collected by distillation. Then the CEC/Fe_3O_4/PFOS material was used to adsorb cyclohexane again.

4.7. Oil/water Separation Experiment. First, 2 mL of oil-red-colored chloroform was dropped into 25 mL of deionized water in a beaker followed by slight shaking to sink the red-colored chloroform in water. The CEC/Fe_3O_4/PFOS material was used to absorb the oil-red-colored chloroform. A similar scheme was used for the treatment of cyclohexane; because the density of cyclohexane is lower than water, so the cyclohexane and CEC/Fe_3O_4/PFOS material float on the water surface. Finally, the CEC/Fe_3O_4/PFOS material can be controlled to touch cyclohexane by a magnet.

For the separation of oil/water mixtures, the CEC/Fe_3O_4/PFOS material was fixed in the funnel stem (12 mm in diameter, 23 mm in height) of the funnel (Figure S5). First, the oil/water mixture solution remained on top of the CEC/Fe_3O_4/PFOS material. Then the solution of penetrating material was collected by gravity action.

Cyclohexane was substituted the disuse oil. The cyclohexane/water emulsion was separated by the CEC/Fe_3O_4/PFOS material. First, 5 mL of cyclohexane and 0.05 g of Tween-80 were dissolved in 30 mL of water. Then the mixture was sonicated for 30 min to prepare a milky emulsion. The obtained emulsion was stable for 24 h. Then the emulsion was poured into the beaker containing the CEC/Fe_3O_4/PFOS material and stirred for 1 min. After that, the CEC/Fe_3O_4/PFOS material was removed. Finally, the solutions of before and after separation were observed by a microscope.

4.8. Characterization of the CEC/Fe_3O_4/PFOS Material. Mercury intrusion porosimetry (MIP, PoreMaster-33 GT, America Quantachrome Corporation, America) was used to measure the porosity, specific surface area, and the pore diameter of the CEC/Fe_3O_4/PFOS material. Scanning electron microscopy (SEM, EVO 18, Germany Electronics Corporation, Germany) equipped with energy dispersive spectroscopy (EDS) was used to measure the appearance of Fe_3O_4, carbonaceous

https://dx.doi.org/10.1021/acsomega.0c00200
ACS Omega 2020, 5, 9920−9928

E.C., and CEC/Fe_3O_4/PFOS material. Magnetic studies of Fe_3O_4 and CEC/Fe_3O_4/PFOS material were measured on a SQUID Magnetic Property Measurement System (Quantum Design, MPMS-XL-7) at ambient conditions. To confirm that Fe_3O_4 and PFOS could be modified on carbonaceous E.C., Fourier transform infrared spectrometer (FT-IR) measurements (VERTEX80, Bruker, Germany) were used to analyze Fe_3O_4, carbonaceous E.C., PFOS, CEC/Fe_3O_4, and CEC/Fe_3O_4/PFOS material; the experiments were performed by the attenuated total reflection mode with the wave numbers from 400 to 4000 cm^{-1}.

■ ASSOCIATED CONTENT

Supporting Information

The Supporting Information is available free of charge at https://pubs.acs.org/doi/10.1021/acsomega.0c00200.

Morphologies of the samples; characterization of the samples SEM images showing the morphologies of CEC/Fe_3O_4/PFOS material; contact angle measurements of the CEC/Fe_3O_4/PFOS material: sliding angles and static contact angles; digital image of the separation device (PDF)

Hydrophobic properties (Movie S1)

Trichloromethane absorption experiment (Movie S2)

Cyclohexane absorption experiment (Movie S3)

■ AUTHOR INFORMATION

Corresponding Author

Chengyong Li − *School of Chemistry and Environment, Guangdong Ocean University, Southern Marine Science and Engineering Guangdong Laboratory, Zhanjiang 524088, China; Shenzhen Institute of Guangdong Ocean University, Shenzhen 518108, China;* orcid.org/0000-0003-0018-165X; Email: cyli@gdou.edu.cn; Fax: +86-759-2383636

Authors

Ruikun Sun − *School of Chemistry and Environment, Guangdong Ocean University, Southern Marine Science and Engineering Guangdong Laboratory, Zhanjiang 524088, China*

Lei He − *School of Chemistry and Environment, Guangdong Ocean University, Southern Marine Science and Engineering Guangdong Laboratory, Zhanjiang 524088, China*

Qingtong Shang − *School of Chemistry and Environment, Guangdong Ocean University, Southern Marine Science and Engineering Guangdong Laboratory, Zhanjiang 524088, China*

Shiqi Jiang − *School of Chemistry and Environment, Guangdong Ocean University, Southern Marine Science and Engineering Guangdong Laboratory, Zhanjiang 524088, China; Shenzhen Institute of Guangdong Ocean University, Shenzhen 518108, China*

Chunxia Zhou − *School of Chemistry and Environment, Guangdong Ocean University, Southern Marine Science and Engineering Guangdong Laboratory, Zhanjiang 524088, China; Shenzhen Institute of Guangdong Ocean University, Shenzhen 518108, China*

Pengzhi Hong − *School of Chemistry and Environment, Guangdong Ocean University, Southern Marine Science and Engineering Guangdong Laboratory, Zhanjiang 524088, China; Shenzhen Institute of Guangdong Ocean University, Shenzhen 518108, China*

Hui Zhao − *School of Chemistry and Environment, Guangdong Ocean University, Southern Marine Science and Engineering Guangdong Laboratory, Zhanjiang 524088, China*

Shengli Sun − *School of Chemistry and Environment, Guangdong Ocean University, Southern Marine Science and Engineering Guangdong Laboratory, Zhanjiang 524088, China*

Complete contact information is available at: https://pubs.acs.org/10.1021/acsomega.0c00200

Notes

The authors declare no competing financial interest.

■ ACKNOWLEDGMENTS

This work was supported by Southern Marine Science and Engineering Guangdong Laboratory (Zhanjiang) (ZJW-2019-07, ZJW-2019-08), Guangdong Yangfan Program (201635018), Guangdong Special Support Program (2017TQ04N706), Science and Technology Planning Project of Zhanjiang City (2018A02014), Special Funds for Science Technology Innovation and Industrial Development of Shenzhen Dapeng New District (KY20180202, PT202001-18), and Innovation and Development Project about Marine Economy Demonstration of Zhanjiang City (2017C8B1).

■ REFERENCES

(1) Xue, J. L.; Grift, T. E.; Hansen, A. C. Effect of Biodiesel on Engine Performances and Emissions. *Renewable Sustainable Energy Rev.* **2011**, *15*, 1098−1116.

(2) Balat, M.; Balat, H. Recent Trends in Global Production and Utilization of Bio-ethanol Fuel. *Appl. Energy* **2009**, *86*, 2273−2282.

(3) Chang, Z.; Sun, Y.; Xu, J.; Zong, X.; Tang, Q.; Guo, L.; Ren, L.; Cheng, W.-H. Hydrophobic Nanostructures Fabricated by Ferric Nitrate Etching Method on Single Crystalline Silicon Surface. *Colloids Surf., A* **2019**, *583*, No. 123999.

(4) Shin, J. H.; Heo, J.-H.; Jeon, S.; Park, J. H.; Kim, S.; Kang, H.-W. Bio-inspired Hollow PDMS Sponge for Enhanced Oil-water Separation. *J. Hazard. Mater.* **2019**, *365*, 494−501.

(5) Vazirinasab, E.; Maghsoudi, K.; Jafari, R.; Momen, G. A Comparative Study of the Icephobic and Self-cleaning Properties of Teflon Materials Having Different Surface Morphologies. *J. Mater. Process. Technol.* **2020**, *276*, No. 116415.

(6) Burton, Z.; Bhushan, B. Surface Characterization and Adhesion and Friction Properties of Hydrophobic Leaf Surfaces. *Ultramicroscopy* **2006**, *106*, 709−719.

(7) Kim, J. S.; Girard, A.; Jun, S.; Lee, J.; You, S. M. Effect of Surface Roughness on Pool Boiling Heat Transfer of Water on Hydrophobic Surfaces. *Int. J. Heat Mass Transfer* **2018**, *118*, 802−811.

(8) Liu, Y.; Peng, Y.; Zhang, T.; Qiu, F.; Yuan, D. Superhydrophobic, Ultralight and Flexible Biomass Carbon Aerogels Derived from Sisal Fibers for Highly Efficient Oil-water Separation. *Cellulose* **2018**, *25*, 3067−3078.

(9) Liu, Y.; Shi, T.; Zhang, T.; Yuan, D.; Peng, Y.; Qiu, F. Cellulose-derived Multifunctional Nano-CuO/carbon Aerogel Composites as a Highly Efficient Oil Absorbent. *Cellulose* **2019**, *26*, 5381−5394.

(10) Chen, Y.; Zhang, X.; Chen, W.; Yang, H.; Chen, H. The Structure Evolution of Biochar from Biomass Pyrolysis and Its Correlation with Gas Pollutant Adsorption Performance. *Bioresource Technol.* **2017**, *246*, 101−109.

(11) Yuan, D.; Zhang, T.; Guo, Q.; Qiu, F.; Yang, D.; Ou, Z. Superhydrophobic Hierarchical Biomass Carbon Aerogel Assembled with TiO_2 Nanorods for Selective Immiscible Oil/Water Mixture and Emulsion Separation. *Ind. Eng. Chem. Res.* **2018**, *57*, 14758−14766.

(12) Yuan, D.; Zhang, T.; Guo, Q.; Qiu, F.; Yang, D.; Ou, Z. Recyclable Biomass Carbon@SiO_2@MnO_2 Aerogel with Hierarchical Structures for Fast and Selective Oil-water Separation. *Chem. Eng. J.* **2018**, *351*, 622−630.

(13) Li, L.; Hu, T.; Sun, H.; Zhang, J.; Wang, A. Pressure-Sensitive and Conductive Carbon Aerogels from Poplars Catkins for Selective Oil Absorption and Oil/Water Separation. *ACS Appl. Mater. Interfaces* **2017**, *9*, 18001−18007.
(14) Dutta, S.; Bhaumik, A.; Wu, K. C. W. Hierarchically Porous Carbon Derived from Polymers and Biomass: Effect of Interconnected Pores on Energy Applications. *Energy Environ. Sci.* **2014**, *7*, 3574−3592.
(15) Zhang, X.; Wang, H.; Cai, Z.; Yan, N.; Liu, M.; Yu, Y. Highly Compressible and Hydrophobic Anisotropic Aerogels for Selective Oil/Organic Solvent Absorption. *ACS Sustainable Chem. Eng.* **2019**, *7*, 332−340.
(16) Wang, L.; Zhang, Q.; Chen, S.; Xu, F.; Chen, S.; Jia, J.; Tan, H.; Hou, H.; Song, Y. Electrochemical Sensing and Biosensing Platform Based on Biomass-Derived Macroporous Carbon Materials. *Anal. Chem.* **2014**, *86*, 1414−1421.
(17) Wu, X.-L.; Wen, T.; Guo, H.-L.; Yang, S.; Wang, X.; Xu, A.-W. Biomass-Derived Sponge-like Carbonaceous Hydrogels and Aerogels for Supercapacitors. *ACS Nano* **2013**, *7*, 3589−3597.
(18) Zhang, Y. Y.; Zhang, D. Y.; Barrett, S. C. H. Genetic uniformity Characterizes the Invasive Spread of Water Hyacinth (*Eichhornia crassipes*), A Clonal Aquatic Plant. *Mol. Ecol.* **2010**, *19*, 1774−1786.
(19) Villamagna, A. M.; Murphy, B. R. Ecological and Socio-economic Impacts of Invasive Water Hyacinth (*Eichhornia crassipes*): A Review. *Freshwater Biol.* **2010**, *55*, 282−298.
(20) Shackleton, R. T.; Biggs, R.; Richardson, D. M.; Larson, B. M. H. Social-ecological Drivers and Impacts of Invasion-related Regime Shifts: Consequences for Ecosystem Services and Human Wellbeing. *Environ. Sci. Policy* **2018**, *89*, 300−314.
(21) Yu, H.; Dong, X.; Yu, D.; Liu, C.; Fan, S. Effects of Eutrophication and Different Water Levels on Overwintering of *Eichhornia crassipes* at the Northern Margin of Its Distribution in China. *Front. Plant Sci.* **2019**, *10*, No. 1261.
(22) Kriticos, D. J.; Brunel, S. Assessing and Managing the Current and Future Pest Risk from Water Hyacinth, (*Eichhornia crassipes*), an Invasive Aquatic Plant Threatening the Environment and Water Security. *PLoS One* **2016**, *11*, No. 0120054.
(23) Liu, D.; Wang, R.; Gordon, D. R.; Sun, X.; Chen, L.; Wang, Y. Predicting Plant Invasions Following China's Water Diversion Project. *Environ. Sci. Technol.* **2017**, *51*, 1450−1457.
(24) Li, Q.; Zhan, J.; Chen, B.; Meng, X.; Pan, X. Removal of Pb, Zn, Cu, and Cd by Two Types of *Eichhornia crassipes*. *Environ. Eng. Sci.* **2016**, *33*, 88−97.
(25) El-Zawahry, M. M.; Abdelghaffar, F.; Abdelghaffar, R. A.; Mashaly, H. M. Functionalization of the Aquatic Weed Water Hyacinth *Eichhornia crassipes* by Using Zinc Oxide Nanoparticles for Removal of Organic Dyes Effluent. *Fibers Polym.* **2016**, *17*, 186−193.
(26) Üner, O.; Bayrak, Y. The Effect of Carbonization Temperature, Carbonization Time and Impregnation Ratio on the Properties of Activated Carbon Produced from *Arundo donax*. *Microporous Mesoporous Mater.* **2018**, *268*, 225−234.
(27) Qu, M.; Ma, L.; Wang, J.; Zhang, Y.; Zhao, Y.; Zhou, Y.; Liu, X.; He, J. Multifunctional Superwettable Material with Smart pH Responsiveness for Efficient and Controllable Oil/Water Separation and Emulsified Wastewater Purification. *ACS Appl. Mater. Interfaces* **2019**, *11*, 24668−24682.
(28) He, F. A.; Fan, J. T.; Ma, D.; Zhang, L. M.; Leung, C.; Chan, H. L. The Attachment of Fe_3O_4 Nanoparticles to Graphene Oxide by Covalent Bonding. *Carbon* **2010**, *48*, 3139−3144.
(29) Yang, C.; Han, N.; Han, C.; Wang, M.; Zhang, W.; Wang, W.; Zhang, Z.; Li, W.; Zhang, X. Design of A Janus F-TiO_2@PPS Porous Membrane with Asymmetric Wettability for Switchable Oil/Water Separation. *ACS Appl. Mater. Interfaces* **2019**, *11*, 22408−22418.
(30) Li, Y.-N.; Hao, Y.-C.; Ye, H.; Zhang, Y.-Z.; Chen, Y.; Xu, X.-J. Single-sided Superhydrophobic Fluorinated Silica/poly (ether sulfone) Membrane for SO_2 Absorption. *J. Membr. Sci.* **2019**, *580*, 190−201.
(31) Qi, S.; Briana, A.; Perman, J. A.; Taylor, B.; Feng-Shou, X.; Shengqian, M. Integrating Superwettability within Covalent Organic Frameworks for Functional. *Coat. Chem.* **2018**, *4*, 1726−1739.
(32) Li, Y. Q.; Samad, Y. A.; Polychronopoulou, K.; Alhassan, S. M.; Liao, K. Carbon Aerogel from Winter Melon for Highly Efficient and Recyclable Oils and Organic Solvents Absorption. *ACS Sustainable Chem. Eng.* **2014**, *2*, 1492−1497.
(33) Lu, Y.; Niu, Z.; Yuan, W. Multifunctional Magnetic Superhydrophobic Carbonaceous Aerogel with Micro/nano-scale Hierarchical Structures for Environmental Remediation and Energy Storage. *Appl. Surf. Sci.* **2019**, *480*, 851−860.
(34) Ma, Q.; Cheng, H. F.; Fane, A. G.; Wang, R.; Zhang, H. Recent Development of Advanced Materials with Special Wettability for Selective Oil/Water Separation. *Small* **2016**, *12*, 2186−2202.
(35) Wang, B.; Liang, W.; Guo, Z.; Liu, W. Biomimetic Superlyophobic and Super-lyophilic Materials Applied for Oil/water Separation: A New Strategy Beyond Nature. *Chem. Soc. Rev.* **2015**, *44*, 336−361.
(36) Zhou, J.; Sun, Z.; Chen, M.; Wang, J.; Qiao, W.; Long, D.; Ling, L. Macroscopic and Mechanically Robust Hollow Carbon Spheres with Superior Oil Adsorption and Light-to-Heat Evaporation Properties. *Adv. Funct. Mater.* **2016**, *26*, 5368−5375.
(37) Kollarigowda, R. H.; Abraham, S.; Montemagno, C. D. Antifouling Cellulose Hybrid Biomembrane for Effective Oil/Water Separation. *ACS Appl. Mater. Interfaces* **2017**, *9*, 29812−29819.
(38) Yue, X.; Zhang, T.; Yang, D.; Qiu, F.; Li, Z. Hybrid Aerogels Derived from Banana Peel and Waste Paper for Efficient Oil Absorption and Emulsion Separation. *J. Cleaner Prod.* **2018**, *199*, 411−419.
(39) Yin, T. T.; Zhang, X. Y.; Liu, X. Y.; Li, B. B.; Wang, C. Q. Cellulose-based Aerogel from *Eichhornia crassipes* as An Oil Superabsorbent. *RSC Adv.* **2016**, *6*, 98563−98570.
(40) Jiang, J.; Zhang, Q.; Zhan, X.; Chen, F. R. Biomass-Derived, Honeycomblike Aerogel As a Robust Oil Absorbent with Two-Way Reusability. *ACS Sustainable Chem. Eng.* **2017**, *5*, 10307−10316.
(41) He, J.; He, J.; Yuan, M.; Xue, M.; Ma, X.; Hou, L.; Zhang, T.; Liu, X.; Qu, M. Facile Fabrication of Eco-Friendly Durable Superhydrophobic Material from Eggshell with Oil/Water Separation Property. *Adv. Eng. Mater.* **2018**, *20*, No. 1701180.
(42) Bi, H.; Huang, X.; Wu, X.; Cao, X.; Tan, C.; Yin, Z.; Lu, X.; Sun, L.; Zhang, H. Carbon Microbelt Aerogel Prepared by Waste Paper: An Efficient and Recyclable Sorbent for Oils and Organic Solvents. *Small* **2014**, *10*, 3544−3550.
(43) Bi, H.; Yin, Z.; Cao, X.; Xie, X.; Tan, C.; Huang, X.; Chen, B.; Chen, F.; Yang, Q.; Bu, X.; Lu, X.; Sun, L.; Zhang, H. Carbon Fiber Aerogel Made from Raw Cotton: A Novel, Efficient and Recyclable Sorbent for Oils and Organic Solvents. *Adv. Mater.* **2013**, *25*, 5916−5921.
(44) Lee, Y. S.; Lee, H. B.; Koo, H. Y.; Choi, W. S. Remote-Controlled Magnetic Sponge Balls and Threads for Oil/Water Separation in a Confined Space and Anaerobic Reactions. *ACS Appl. Mater. Interfaces* **2019**, *11*, 40886−40897.

https://dx.doi.org/10.1021/acsomega.0c00200
ACS Omega 2020, 5, 9920−9928